


Relevance of Cu-3*d* multiplet structure in models of high-*T_c* cuprates

Mi Jiang , Mirko Moeller, Mona Berciu, and George A. Sawatzky

*Department of Physics and Astronomy, University of British Columbia, Vancouver B.C., Canada V6T 1Z1
and Stewart Blusson Quantum Matter Institute, University of British Columbia, Vancouver B.C., Canada V6T 1Z4*



(Received 13 July 2019; revised manuscript received 10 January 2020; published 31 January 2020)

We revisit the problem of the spectra of two holes in a CuO₂ layer, modeled as a Cu-3*d*⁸ impurity with full multiplet structure coupled to a full O-2*p* band as an approximation to the local electronic structure of a hole-doped cuprate. Unlike previous studies that treated the O band as a featureless bath, we describe it with a realistic tight-binding model. While our results are in qualitative agreement with previous work, we find considerable quantitative changes when using the proper O-2*p* band structure. We also find that (i) the ligand O-2*p* orbitals play an essential role, within this impurity model; (ii) the three-orbital Emery model provides an accurate description for the subspace with ¹A₁ symmetry, which includes the ground state in the relevant region of the phase diagram; (iii) this ground state has only ~50% overlap with a Zhang-Rice singlet; (iv) there are other low-energy states, in subspaces with different symmetries, that are absent from the three-orbital Emery model and its one-band descendants. These states play an important role in describing the elementary excitations of doped cuprates.

DOI: [10.1103/PhysRevB.101.035151](https://doi.org/10.1103/PhysRevB.101.035151)

I. INTRODUCTION

A central issue still under debate in the study of high-*T_c* cuprate superconductors is the proper minimal model that correctly captures the low-energy properties, specifically the precise nature of the states closest to the Fermi level. Historically, Anderson proposed that the essential physics can be understood based on the single-band Hubbard model, where the band is identified as the antibonding band of Cu-3*d*_{x²-y²} and O-2*p* orbitals [1]. The even simpler *t*-*J* model additionally discards all doubly occupied states and describes a square lattice where charge carriers move in a spin background. This model has been extensively studied and is believed to provide a good description of the Hubbard model in the strong coupling limit $J/t = 4t/U \ll 1$. However, their common intrinsic assumption is that the cuprate parents compounds, which are charge-transfer insulators [2], can instead be modeled as effective Mott-Hubbard insulators.

The need to understand the importance of explicitly including the O ions hosting the doped holes motivated the study of the three-band Emery model [3], which includes the Cu-*d*_{x²-y²} and the two ligand O-2*p*_σ orbitals in the nonmagnetic unit cell. The key idea underlying the expected equivalence of the one- and three-orbital scenarios was proposed by Zhang and Rice, who argued that the doped holes occupy the ¹A₁ linear combination of O orbitals, and are locked into a Zhang-Rice singlet (ZRS) with the hole (spin) residing on the central Cu site. Projecting onto these ZRS then allows one to map the three-band Emery model onto a single-band *t*-*J* model [4], although a more careful treatment reveals the existence of additional terms ignored by the *t*-*J* Hamiltonian [5,6].

Although various analytical approximations and extensive numerical studies of these model Hamiltonians have revealed many insights in the past decades, the validity of the ZRS concept [7,8] and more generally the equivalence,

or lack thereof, between the low-energy properties of one- and three-orbital models are still under debate. On one hand, the existence and stability of states with ZRS-like character have been confirmed in previous photoemission experiments [9–11]. On the other hand, recent calculations contrasting the dynamics of a single doped hole in the one-band vs the three-band model revealed qualitative differences [12–14], such as the essential vs the minor role played by the background spin fluctuations, respectively. Moreover, a recent high-energy optical conductivity study questioned the ZRS argument by revealing a strong mixture of singlet and triplet configurations in the lightly hole-doped Zn-LSCO single crystal [7]. Furthermore, this system exhibits strong ferromagnetic correlations between Cu spins near the doped holes, as predicted by the three-band model [12].

During the same period when the ZRS was proposed, Eskes *et al.* carried out a more general study that included the multiplet structure of the Cu, i.e., all singlet and triplet irreducible representations in the *D*_{4h} point group spanned by two *d* holes (*d*⁸-type configurations) and their corresponding Coulomb and exchange interactions [15–17], aside from explicitly considering the O band. This was achieved at the cost of simplifying the model to consist of a single Cu impurity hybridizing with a broad O band described in terms of a featureless, semielliptical density of states.

This work confirmed that the first ionization state starting from a Cu-*d*⁹ state and a full O-2*p* band, which ends with the two hole eigenstates involving *d*⁸ multiplets and various continuum states, is indeed in the ¹A₁ symmetry channel consistent with the symmetry of the ZRS, but also found that the energy difference between the lowest ionization states for various symmetry channels is rather small. Moreover, these differences are strongly dependent on the electronic structure, which in turn is likely to depend quite strongly on doping levels. These results cast doubt on whether it suffices to

include only the $d_{x^2-y^2}$ orbital instead of the full $3d$ multiplet structure of the Cu- d^8 , when modeling these materials.

Most members of our community believe that the Cu- $d_{x^2-y^2}$ orbital is the only d orbital needed to account for the essential physics of cuprates, explaining why there are so few studies on the effects of the multiplet structure, compared to the very extensive investigations of the one- and three-band models involving only Cu- $d_{x^2-y^2}$ orbital and/or its ZRS daughter. However, there are both theoretical and experimental results pointing out the importance of nonplanar orbitals like Cu- $3d_{3z^2-r^2}$ and/or O- $2p_z$ [18–30]. In particular, the importance of Cu- $3d_{3z^2-r^2}$ is revealed by the recent discovery [30] of the cuprate superconductor Ba₂CuO_{4- δ} with critical temperature $T_c \sim 70$ K, where based on the compressed c -axis bond length, it is claimed that some doped holes are likely in the $d_{3z^2-r^2}$ orbital. Early Auger spectroscopic experiments [31] clearly demonstrated strong multiplet effects ranging over a large energy scale in Cu compounds such as CuO and Cu₂O. In fact, in Cu₂O the lowest-energy Cu- d^8 state is a triplet state consistent with the Hund’s rule expectations. As pointed out by Eskes [15,16], the crossing of the singlet and triplet states in the cuprate parent compounds is a result of the strong O character in these states due to the strong Cu-O hybridization and the fact that bound states with Cu- d^8 character are pushed out of the top of the O- $2p$ band, resulting in the lowest-energy singlet bound state [9,10,31].

More important evidence for the role of the multiplets comes from x-ray absorption (XAS) experiments that have shown, upon increased doping, a strong change from purely x, y polarized absorption to one including a large contribution of z polarized intensity for the O and Cu core-to-valence transition [19]. This implies that there are doped holes whose wave functions have a considerable component in the Cu- $d_{3z^2-r^2}$ or O- p_z orbitals. These results point to the breakdown of the single-band or even three-band (Cu- $d_{x^2-y^2}$ based) approaches to the description of the phase diagram of cuprate superconductors.

This motivates us to revisit the importance of the full Cu- $3d$ multiplet structure and explore its effects on the low-energy properties of cuprate models. In order to obtain numerically exact results, we follow Eskes *et al.* and study a single Cu impurity with all its $3d$ orbitals included. In contrast to this earlier work, however, we properly embed this Cu impurity in a square lattice of O- $2p$ orbitals, with a realistic band structure. This allows us to contrast models containing only the O- $2p$ ligand orbitals vs those also including the other in-plane orbital, and also the p_z orbital. It is important to note that the linear combination of O- $2p$ orbitals that hybridize with the various Cu- $3d$ states live in different energy regions of the realistic O- $2p$ band structure and this strongly influences the importance of this hybridization. For example, the d_{xz} orbital hybridizes with the O- p_z and p_x π -bonding orbitals while the $d_{x^2-y^2}$ orbital hybridizes with the O- $2p$ σ -bonding orbitals. Besides, the linear combination of the O- $2p$ orbitals that hybridize with $d_{x^2-y^2}$ orbital is different in their relative phases than with the $d_{3z^2-r^2}$ orbital. We show below that this strongly influences the stability and relative energies of the bound states pushed out of the O band for the various symmetries. Our results reveal the importance of the realistic modeling of the O bath, and which O- $2p$ play an

essential role. This is a lesson of broad relevance to the field, given the increased use of impurity-based calculations such as dynamical mean-field theory (DMFT) for the modeling of materials. Clearly, realistic descriptions of the baths are essential for obtaining accurate results.

Furthermore, by calculating the Cu- $3d$ electron removal spectra in various symmetry channels of the D_{4h} point group, we are able to identify the character (symmetry, spin, and orbital composition) of the first ionization state, and to gauge its similarity to a ZRS. Finally, our results reveal strong similarities between the model including all multiplets and the conventional three-orbital Emery model if we restrict ourselves to the lowest-energy electron removal states, although open issues still remain. However, if one wants to describe spectroscopies like ARPES going up to one or more eV below the Fermi energy as, for example, in descriptions of the so-called “waterfall” feature [32], it is essential to include all of the multiplets since they all have appreciable spectral weights extending to energies well above 1 eV.

This paper is organized as follows. In Sec. II, we define our model and the variational method employed to study its single-doped hole eigenstates. Section III discusses the resulting spectra for various cases considered. The summary and future issues to be addressed are presented in Sec. IV.

II. MODELS AND METHODS

Multiorbital models with a single Cu impurity

We simplify the description of a CuO₂ plane by replacing the Cu lattice with a single Cu impurity properly embedded in a square lattice of O orbitals; the resulting problem can be solved exactly, unlike the corresponding one for the full CuO₂ lattice. The central part of the system, consisting of the Cu impurity and its four nearest-neighbor (NN) O ions, is depicted in Fig. 1. The Hamiltonian describing this system is

$$\begin{aligned}
 H &= E_s + K_{pd} + K_{pp} + V_{dd} + V_{pp}, \\
 E_s &= \sum_{m\sigma} \epsilon_d(m) d_{m\sigma}^\dagger d_{m\sigma} + \sum_{jn\sigma} \epsilon_p p_{jn\sigma}^\dagger p_{jn\sigma}, \\
 K_{pd} &= \sum_{(j)m\sigma} (T_{mn}^{pd} d_{m\sigma}^\dagger p_{jn\sigma} + \text{H.c.}), \\
 K_{pp} &= \sum_{(j')m'\sigma} (T_{m'n'}^{pp} p_{jn\sigma}^\dagger p_{j'n'\sigma} + \text{H.c.}), \\
 V_{dd} &= \sum_{\bar{m}_1\bar{m}_2\bar{m}_3\bar{m}_4} U(\bar{m}_1\bar{m}_2\bar{m}_3\bar{m}_4) d_{\bar{m}_1}^\dagger d_{\bar{m}_2} d_{\bar{m}_3}^\dagger d_{\bar{m}_4}. \quad (1)
 \end{aligned}$$

In V_{dd} we use the shorthand notation $\bar{m}_x \equiv m_x \sigma_x$, with $x = 1, \dots, 4$ denoting spin orbitals. E_s are the onsite energies, where $d_{m\sigma}^\dagger$ ($d_{m\sigma}$) creates (destroys) a hole in the Cu- $3d$ orbital m with onsite energy $\epsilon_d(m)$ and spin σ , while $p_{jn\sigma}^\dagger$ ($p_{jn\sigma}$) creates (destroys) a hole at the O lattice site j , in its $2p$ orbital n with energy ϵ_p and spin σ . The Cu- $3d$ orbitals indexed by m are $b_1(d_{x^2-y^2})$, $a_1(d_{3z^2-r^2})$, $b_2(d_{xy})$, $e_x(d_{xz})$, $e_y(d_{yz})$, and the O- $2p$ orbitals indexed by n are p_x, p_y, p_z or a subset of them, as indicated below. All other core levels and the Cu- $4s$ and - $4p$ orbitals are neglected because of their high energy, which allows for their influence via hybridization to be accounted

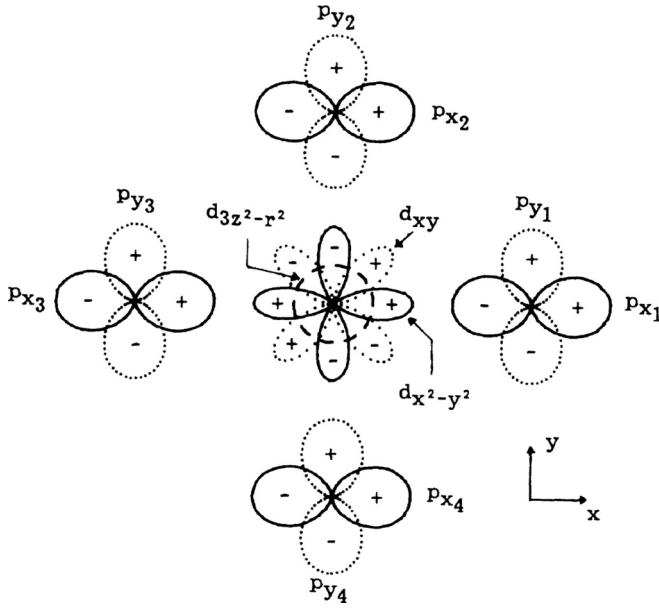


FIG. 1. Schematic view of the orbitals involved in our model calculations, adapted from Eskes's previous related work [16]. The Cu- d_{xz} , d_{yz} and the O- p_z orbitals are not shown. Note that only the four O that are adjacent to the Cu impurity are depicted, however, we consider the full O square lattice.

for by the renormalization of the effective parameters. Finally, the onsite single d -hole energies $\epsilon_d(m) = 0$ are assumed to be independent of m , thus omitting the point-charge crystal splitting. This is expected to be a good approximation because it is the hybridization with the O orbitals, included in our model, that accounts for most of the difference between the effective onsite energies of the $3d$ levels. As a result, the charge-transfer energy $\Delta = \epsilon_p$.

K_{pd} and K_{pp} describe the Cu-O and O-O hoppings, respectively. The labels j, j' run over the positions of the O atoms, $\langle j \rangle$ is a sum over the four O adjacent to the j th Cu site, and only NN pp hopping is included. Following Slater and Koster [33], the Cu-O and O-O hopping integrals T_{mn}^{pd} and T_{mn}^{pp} are listed in Table I of Appendix A. Throughout the paper, energies are measured in eV.

In the following we focus on four possible models: (i) N3, where $m = b_1$ and $n \in \{p_{x_1}, p_{y_2}\}$, i.e., the usual three-band Emery model where only the ligand orbital is kept for each O; (ii) N7, where $m \in \{a_1, b_1, b_2, e_x, e_y\}$ and $n \in \{p_{x_1}, p_{y_2}\}$, i.e., multipletlike physics is added to the Emery model; (iii) N9, where $m \in \{a_1, b_1, b_2, e_x, e_y\}$ and $n \in \{p_{x_1}, p_{y_1}, p_{x_2}, p_{y_2}\}$, i.e., for each O we keep both in-plane $2p$ orbitals; and (iv) N11, where $m \in \{a_1, b_1, b_2, e_x, e_y\}$ and $n \in \{p_{x_1}, p_{y_1}, p_{z_1}, p_{x_2}, p_{y_2}, p_{z_2}\}$, i.e., for each O we keep all three O- $2p$ orbitals.

For the N9 and N11 models we use $T_{b_2}^{pd} = T_{b_1}^{pd}/2$, so that $t_{pd\pi} = \sqrt{3}t_{pd\sigma}/4$. We emphasize that all the Cu-O hybridization parameters $t_{pd}, t_{pp}, t_{pd\sigma}, t_{pd\pi}, t_{pp\sigma}, t_{pp\pi}$ are taken to be positive, and the signs due to the orbitals' overlap (see Fig. 1) are explicitly indicated in Table I of Appendix A.

In this impurity model, the single-electron removal eigenstates of the undoped Cu- d^{10} system are due to the hybridization

of various Cu- d^9 configurations with the full O band $2p^6$, in other words, there is a single hole in the system and the problem can be solved trivially. As expected, if the bottom of the oxygen band at $\Delta - 4t_{pp} > \epsilon_d$, then the lowest-energy electron removal state is dominated by an (antibonding) orbital of b_1 symmetry that has predominantly Cu- d^9 character; this is mixed with ligand hole $d^{10}\underline{L}$ states which have a low amplitude of probability. This confirms that if there is a single hole in the system, it is indeed located primarily on the Cu as in the ground state of the undoped cuprates.

Photoemission or doping of the system with one hole from its ground state of mainly d^9 character removes another electron. The resulting two-hole problem is exactly solvable using the Cini-Sawatzky method [34]. The two-hole problem requires taking into account the Coulomb and exchange interactions $U(\tilde{m}_1\tilde{m}_2\tilde{m}_3\tilde{m}_4)$ described by V_{dd} . These are listed in Appendix A for all singlet/triplet irreducible representations of the D_{4h} point group spanned by two d holes, in terms of the Racah parameters A , B , and C . Throughout the paper, the free-ion values $B = 0.15$ eV, $C = 0.58$ eV are adopted and A is treated as a variable.

If our focus was on relevance to experiments, we would need to calculate the d -electron removal spectrum $A_d^\Gamma(\omega)$ which can be compared to photoemission experiments, and the d^8 partial density of states (PDOS) for the various two-hole irreducible representations (symmetry channels Γ) $A_{d^8}^\Gamma(\omega)$, linked to the resonant photoemission [16]. They are defined by

$$A_d^\Gamma(\omega) = -\frac{1}{\pi} \sum_{mm'} \lim_{\delta \rightarrow 0} \text{Im} G_{dd}(m, m', \omega + i\delta; \Gamma),$$

$$A_{d^8}^\Gamma(\omega) = -\frac{1}{\pi} \sum_{mm'} \lim_{\delta \rightarrow 0} \text{Im} G_{d^8}(m, m', \omega + i\delta; \Gamma) \quad (2)$$

with

$$G_{dd}(m, m', z; \Gamma) = \langle \psi_{g.s.} | d_m^\dagger \hat{G}(z) d_m^\dagger | \psi_{g.s.} \rangle,$$

$$G_{d^8}(m, m', z; \Gamma) = \langle 0 | d_m d_m \hat{G}(z) d_m^\dagger d_m^\dagger | 0 \rangle,$$

$$\hat{G}(z) = (z - \hat{H})^{-1}, \quad z = \omega + i\delta. \quad (3)$$

Here, $|0\rangle$ is the Cu- $3d^{10} + O-2p^6$ state, i.e., the state with no holes, while $|\psi_{g.s.}\rangle$ is the one-hole ground-state.

For our purposes, however, it suffices to obtain their common part, namely, the component of d^8 partial density of states $A^\Gamma(\omega)$ which assumes that one hole has already occupied the b_1 orbital (remember that $d_{b_1}^\dagger |0\rangle$ is the dominant contribution to $|\psi_{g.s.}\rangle$):

$$A^\Gamma(\omega) = -\frac{1}{\pi} \sum_m \lim_{\delta \rightarrow 0} \text{Im} G_d(m, b_1, \omega + i\delta; \Gamma),$$

$$G_d(m, z; \Gamma) = \langle 0 | d_{b_1} d_m \hat{G}(z) d_m^\dagger d_{b_1}^\dagger | 0 \rangle. \quad (4)$$

We focus primarily on $G_d(m, z; \Gamma)$ from now on, but all other propagators $G_{dd}(m, m', z; \Gamma)$ and $G_{d^8}(m, m', z; \Gamma)$ can be calculated similarly. All the calculations are performed by employing the variational exact diagonalization method discussed in Appendix B.

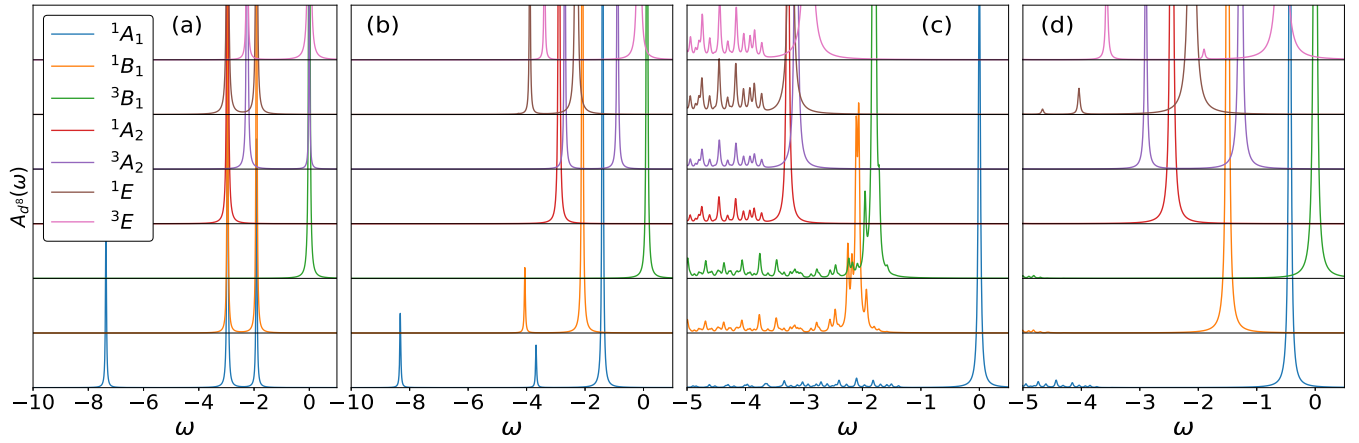


FIG. 2. The two-hole spectra $A^\Gamma(\omega)$ calculated for various irreducible representations Γ in the seven-orbital (N7) model. Panels (a) and (b) are for an isolated Cu- d^8 ion with onsite energies $\epsilon_d(m) = 0$ (a), and with onsite energies $\epsilon_d(m)$ given by the additional point charge crystal fields of Ref. [35] with $A = 6.5$ eV. Panels (c) and (d) are for the Cu impurity that hybridizes with the O lattice, and depict the two characteristic cases of two-hole ground state of 1A_1 (c) and 3B_1 (d) symmetry, respectively. The parameters are (c) $\Delta = 2.75$ eV, $A = 6.5$ eV and (d) $\Delta = 6.5$ eV, $A = 2.5$ eV with $t_{pd} = 1.5$ eV, $t_{pp} = 0.55$ eV. The chemical potential, taken to be zero energy, is chosen as the lowest energy of two-hole state.

III. RESULTS

Before we proceed, we note that throughout the paper we adopt the usual convention of photoemission spectroscopies that the electron removal energy, the hole energy, increases to the left while the energy of the electron addition states increases to the right. The chemical potential, taken to be the zero energy, is chosen at the lowest energy of the two-hole state.

Figure 2 shows the two-hole spectra $A^\Gamma(\omega)$ calculated for various irreducible representations Γ in the N7 model. The first two panels are for an isolated Cu- $3d^8$ when the ligand field splitting is ignored, $\epsilon_d(m) = 0$ [Fig. 2(a)] and when the point charge crystal fields [35] are included [Fig. 2(b)].

If $\epsilon_d(m) = 0$, the two d holes can have 1S , 3P , 1D , 3F , 1G configurations, with energies listed in Ballhausen [36]. As shown in Fig. 2(a), $A_{j^8}^\Gamma(\omega)$ indeed consist of one or more discrete peaks located at these five energies; the number of peaks and their corresponding spectral weights depend on the singlet/triplet nature of the irreducible representation Γ . The inclusion of the point-charge crystal-field splittings [35] in Fig. 2(b) only induces modest shifts of the atomic peaks and modification of their spectral weights. This is why the point-charge crystal fields are ignored from now on.

Hybridization with the O band, shown in Figs. 2(c) and 2(d), results in a significant spreading of the spectral weights over a much wider energy range, and a complete reordering of the low-energy, multipletlike bound states. Indeed, for this realistic value of $t_{pd} = 1.5$ eV, there is no significant correspondence between the bound peak positions and the multiplets in the atomic limit of $t_{pd} = 0$; neither the splittings between the bound peaks, nor even their order, mimic what is found in the atomic multiplet. Instead, of great importance is that for a not too large Δ [Fig. 2(c)], the lowest-energy state is not the expected triplet according to the Hund's rule [Fig. 2(d)] but a singlet state [37].

We first focus on the case illustrated in Fig. 2(c), where the two-hole ground state is of 1A_1 symmetry, like that of the

ZRS. For these parameters, its eigenstate is

$$|\psi\rangle = \sqrt{0.072}|b_1b_1\rangle + \sqrt{0.549}|b_1L_{b_1}\rangle + \sqrt{0.054}|b_1L'_{b_1}\rangle + \sqrt{0.275}|d^{10}L^2\rangle + \dots, \quad (5)$$

where \dots are contributions with a_1a_1, b_2b_2, ee characters, whose probabilities add up to about 5%. Here, L_{b_1} denotes a hole in the linear combination of b_1 symmetry of the four O orbitals nearest to the Cu impurity. We emphasize that this weight is almost independent of the number of orbitals included, i.e., whether we use the N3, N7, N9, or N11 models. This shows that the ground state is only about 55% ZRS like, i.e., $|b_1L_{b_1}\rangle$. L'_{b_1} denotes the configurations where the hole is on the second, third, etc., rings of O ions, which are discarded in the ZRS. The strong mixing with the $d^{10}L^2$ state is the reason for the strong antiferromagnetic exchange interaction which stabilizes the singlet [38].

This lowest bound state of 1A_1 symmetry is separated from the continuum corresponding to the doped hole in the O-2p band by about 1 eV, which is close to what is observed by ARPES experiments in cuprates. In addition to the broadening and appearance of bound states aside from the continua, the hybridization also introduces the ligand fieldlike splittings which will mix the various atomic multiplets. Note that for these parameters, only the 1A_1 peak is clearly below its corresponding continuum, and thus truly a bound state; the other peaks are inside the lower edge of their continua. At even higher energies lies the two-hole continuum, with both holes in the O lattice and the Cu in a d^{10} state; this is superimposed over strong resonances where Cu multiplet lines hybridize with (and are shifted around by) this continuum. All this forms a very broad structure with mixed character and is basically the origin of the so-called “waterfall” [32].

Next, we elaborate on the case where the lowest-energy two-hole ground state is of 3B_1 symmetry, as illustrated in Fig. 2(d). Here we chose $A - \Delta = -4$ eV, which puts the system well into the Mott-Hubbard rather than the

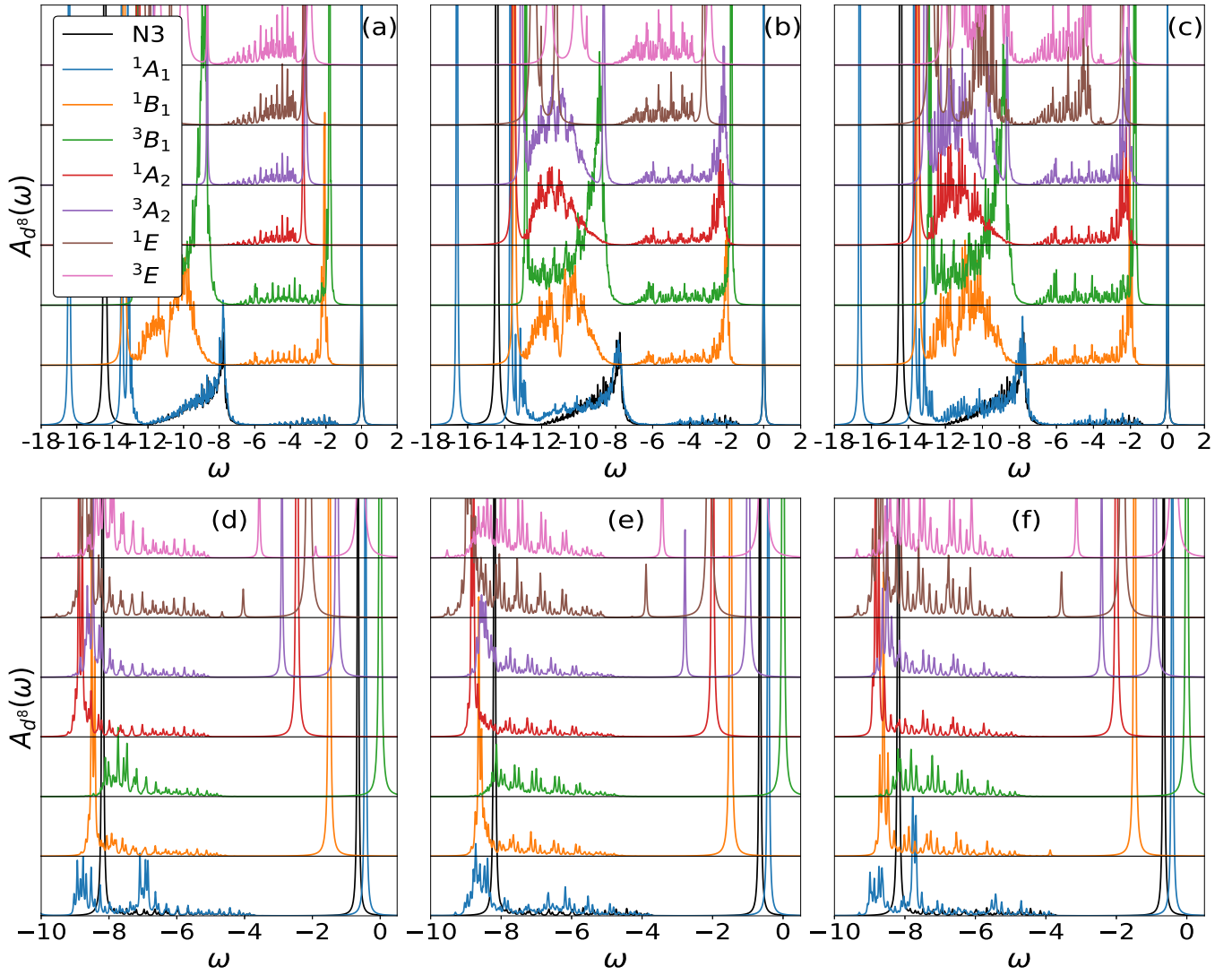


FIG. 3. The comparison of two-hole spectra $A^\Gamma(\omega)$ calculated for various irreducible representations Γ in the (a), (d) 7-orbital (N7), (b), (e) 9-orbital (N9), and (c), (f) 11-orbital (N11) models for two characteristic parameter sets corresponding to the low-spin (singlet) (a)–(c) and high-spin triplet (d)–(f) cases. The spectra of N3 model (black curve) is plotted for comparison as well. The parameters are (a)–(c) $\Delta = 2.75$ eV, $A = 6.5$ eV and (d)–(f) $\Delta = 6.5$ eV, $A = 2.5$ eV with (a), (d) $t_{pd} = 1.5$ eV, $t_{pp} = 0.55$ eV and (b), (c), (e), (f) $t_{pd\sigma} = \sqrt{3}$ eV, $t_{pd\pi} = 0.75$ eV, $t_{pp\sigma} = 0.9$ eV, $t_{pp\pi} = 0.2$ eV. For the N3 model, we use $U_{dd} = A + 4B + 3C$, $t_{pp} = 0.55$ eV.

charge-transfer insulator region in the Zaanen-Sawatzky-Allen (ZSA) classification scheme. The major difference from the case shown in Fig. 2(c) is the order of the lowest peaks, which changed from 1A_1 , 3B_1 , 1B_1 to 3B_1 , 3E , 3A_2 . Furthermore, it is clear that the conventional three-orbital (N3) model cannot capture the lowest bound state any more due to the lack of the involvement of the $a_1(d_{3z^2-r^2})$ orbital.

All these results are qualitatively similar to those reported in previous work by Eskes *et al.* [15,16]. The quantitative differences, especially the differences in the weights of various continua, are due to how the O band is modeled (realistic tight-binding model in our work vs featureless semielliptical DOS in theirs).

To investigate the effects of including more Cu-3d and/or O-2p orbitals in the model Hamiltonians, Fig. 3 compares the two-hole spectra $A^\Gamma(\omega)$ calculated for the (a), (d) 7-orbital (N7), (b), (e) 9-orbital (N9), and (c), (f) 11-orbital (N11) models for two characteristic parameter sets corresponding

to the low-spin singlet (a)–(c) and high-spin triplet (d)–(f) cases. The comparison between N7 and N9/N11 models illustrates the impact of including additional π -bonding oxygen orbitals. The additional hybridization with Cu- $b_2(d_{xy})$ orbital extends the continua to lower energies for all the symmetries involving b_2 , which causes a much smaller difference between the continuum bottom of various A and B types of symmetries. This clearly demonstrates the importance of having all the continua in place correctly in order to decide which is the lowest-energy state. For example, if the 1A_1 continuum would also be involved in the hybridization with the 3B_1 or 1B_1 state, these states would be appreciably closer to the 1A_1 lowest-energy state and even cross it. This could happen if we could take into account the full lattice of Cu- d^9 states in the starting configuration, for example, as done in the exact diagonalization study of a large cluster by Lau *et al.* [12]. It is important to note that Lau found a very strong ferromagnetic coupling between the two Cu's sandwiching an O hole, suggesting that

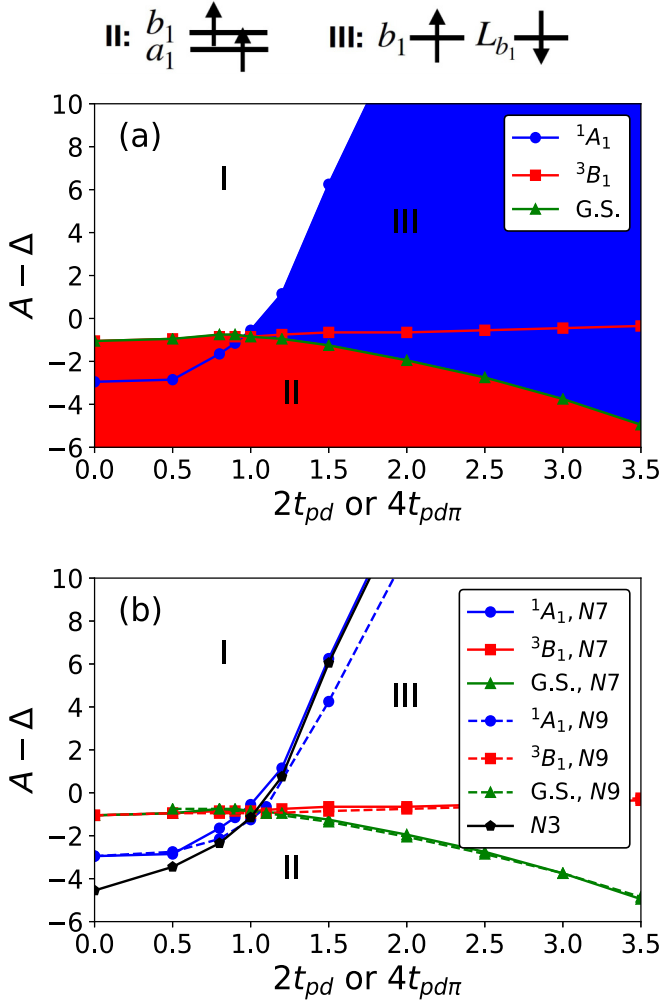


FIG. 4. (a) N7 one-doped hole phase diagram for $\Delta = 2.75$ eV and oxygen bandwidth $W = 4.4$ eV, i.e., $t_{pp} = 0.55$ eV. Region I has no bound state, while in regions II and III and the doped hole is bound to the Cu hole in a complex with 3B_1 and 1A_1 symmetry, respectively. (b) Comparison between N3, N7, and N9 phase diagrams. The conventional relations $t_{pd} \approx \sqrt{3}t_{pd\sigma}/2 = 2t_{pd\pi}$ and $t_{pp\sigma} = 0.9$ eV, $t_{pp\pi} = 0.2$ eV are adopted in the N9 model. For the N3 model, we use $U_{dd} = A + 4B + 3C$, $t_{pp} = 0.55$ eV. The black line denotes the boundary for the appearance of the ZRS-like states in the N3 model. The colored lines indicate the phase boundaries for obtaining a sharp “boundlike state” at low energy with 1A_1 (blue curve) and 3B_1 (red curve) symmetries.

our impurity limit could be different from what happens in the actual crystal (although experiments do agree with our classification for the undoped system). Strong hole doping, however, could strongly modify these conclusions. This also questions the use of single-site DMFT or single-orbital cluster DMFT results with regard to the relevance for the full problem which includes both O and Cu states explicitly.

In the isolated Cu atom, the two-hole ground state has 3B_1 symmetry (Hund’s rule) [see Fig. 2(a)]. As shown in Fig. 2(c), a strong enough hybridization with the O bands favors a ground state with 1A_1 symmetry, i.e., there is a high-spin to low-spin transition. In Fig. 4 we show the ground-state symmetry in the full parameter space. In Fig. 4(a), we

plot a $A - \Delta$ vs $2t_{pd}$ phase diagram, which can be directly compared against that shown in Ref. [15] (a three-dimensional phase diagram is shown in the Appendix). It shows the phase boundaries for obtaining the lowest peak with 1A_1 (blue curve) and with 3B_1 (red curve) symmetries, respectively, for an O bandwidth $W = 4.4$ eV ($t_{pp} = 0.55$ eV). Furthermore, the green curve shows the phase boundary separating the ground state of 1A_1 (low-spin) and 3B_1 (high-spin) character. The three different types of ground states are filled by different colors: region I denotes the absence of a bound ground-state state, i.e., the doped hole moves freely in the O lattice. In regions II and III there is a bound ground state with 3B_1 and 1A_1 symmetry, respectively. Clearly, region III is physically relevant to cuprates.

While this phase diagram is qualitatively similar to Eskes’s corresponding phase diagram [15], there is a shift of the critical value of the pd hybridization needed to obtain a bound state with 1A_1 symmetry from their value $T(B_{1g}) = 2t_{pd} \approx 1.6$ eV to our value of ≈ 1.0 eV. In addition, the lines separating the various regions have quite different slopes. These nontrivial quantitative differences are due to the difference in how the O bath is modeled. In Eskes’s approach [15], the ligand hole states are all spread equally over the hemispherical band while in our tight-binding band structure, the b_1 symmetry hole states are concentrated at the bottom of the (hole) band, which makes the appearance of a two-hole 1A_1 bound state possible at even lower t_{pd} . Another important difference caused by the same effect is that we find a larger splitting between the 1A_1 and the 3B_1 peaks (it is even larger for the 1B_1 case). This results in a stabilization of the 1A_1 state to even more negative $A - \Delta$, extending even further into the Mott-Hubbard regime of the ZSA classification scheme.

For cuprates, the fact that our accurate modeling of the O band leads to a shift in the location of the boundary separating ground states with 1A_1 (low spin $S = 0$) vs 3B_1 (high spin $S = 1$) is irrelevant, as they lie deeply within the charge-transfer insulator regime. However, for materials that fall in the crossover regime, accurate modeling is important. Using a simplified featureless O band may result in the wrong identification of the nature of the ground state. In this crossover region, the choice as to whether the first electron removal state favors the high- or the low-spin ground state depends sensitively on parameters, which themselves depend on the details of the lattice structure. The t_{pd} hopping integrals, in particular, are very sensitive to the interatomic distances so applying pressure could lead to a switch from one type of ground state to the other. Such behavior will be completely missed by too simplistic modeling.

Figure 4(b) illustrates the impact of the number of O- $2p$ orbitals kept in the model on the phase boundaries. The conventional relations $t_{pd} \approx \sqrt{3}t_{pd\sigma}/2 = 2t_{pd\pi}$ and $t_{pp\sigma} = 0.9$ eV, $t_{pp\pi} = 0.2$ eV are used for the N9 model. Clearly, adding the second in-plane O- $2p$ orbital in the model does not have significant effects, except to slightly shift the I-III boundary. The same is true if the p_z orbitals are also included, in N11 (not shown). For comparison, the black line denotes the critical $A - \Delta$ for the appearance of low-energy bound state of Zhang-Rice singlet nature in the N3 model. At larger t_{pd} this agrees well with the 1A_1 boundary for N7

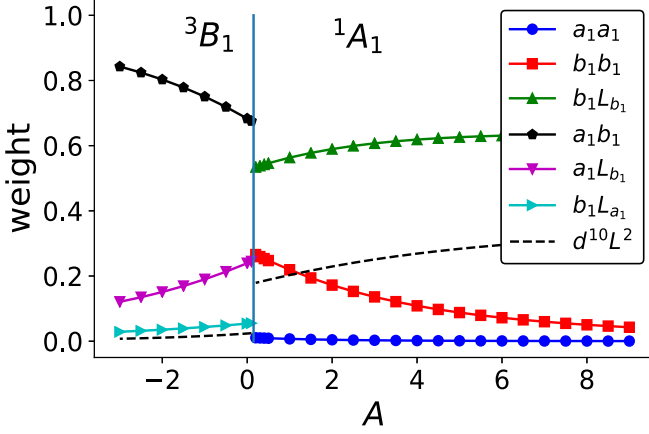


FIG. 5. Variation of the ground-state weights of the dominant components versus A , for fixed $t_{pd} = 1.5$ eV, $\Delta = 3.5$ eV. The vertical line denotes the critical value $A = 0.1$ eV separating the two phases.

model, suggesting minor differences there between the N3 and N7 models.

To further characterize the evolution of the ground state from region II (3B_1) to III (1A_1), Fig. 5 plots how the weights of the dominant components to the ground state change with A , for realistic values of $t_{pd} = 1.5$ eV, $\Delta = 3.5$ eV. As expected [see also Eq. (5)], in region III the ground state is dominated by the $b_1L_{b_1}$ singlet, which is the equivalent of the ZRS. In region II, the high-spin ground state is dominated by the a_1b_1 triplet. However, in both cases there are significant contributions from other configurations with the correct symmetry. This shows that overly simplistic models, which project out everything but the largest probability component, may be qualitatively correct but will certainly not be quantitatively accurate for realistic values of the parameters.

Finally, we provide the detailed comparison between the results of the conventional three-orbital Emery model (N3 in our notation) against the N7 and N9 results to see if the multiplet physics plays any essential role at values of the parameters believed to be reasonable for cuprates. To achieve this, we performed the N3 calculation with the same Cu-O hybridization, O-2p hopping integrals, and charge-transfer energy Δ in region III of the phase diagram as in the N7 model, but keeping only the $b_1(d_{x^2-y^2})$ orbital with a Hubbard-type $U_{dd} = A + 4B + 3C$ (see Table II of Appendix A).

Figure 6(a) compares the spectral weight of 1A_1 symmetry for the three models. Clearly, the ground-state peak and the intermediate energy continua due to Cu-O hybridization are in good agreement. However, the high-energy regions ($\omega \approx 10.0$ eV) of the N7 and N9 models differ from that of the N3 model, as the latter has a double-occupancy peak at about U_{dd} instead of the full multiplet spectrum of the former. Figures 6(b) and 6(c) focus on the ground-state energy and peak weight, respectively. The models are in very good agreement, suggesting that multiplet physics and/or inclusion of nonligand O-2p orbitals has little relevance for the nature of the ground state. These results appear to confirm the validity of the conventional three-orbital Emery model for describing the low-energy physics of the cuprates.

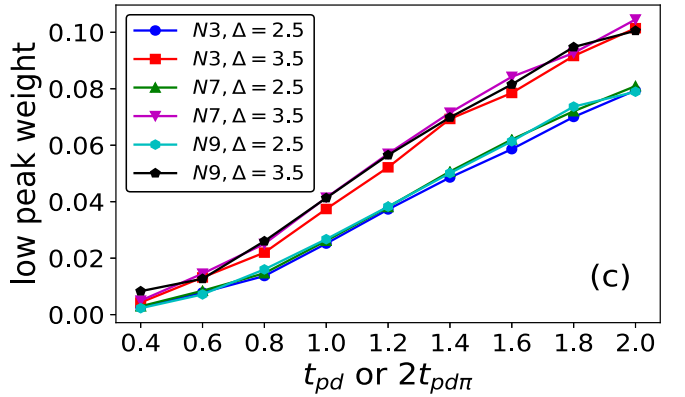
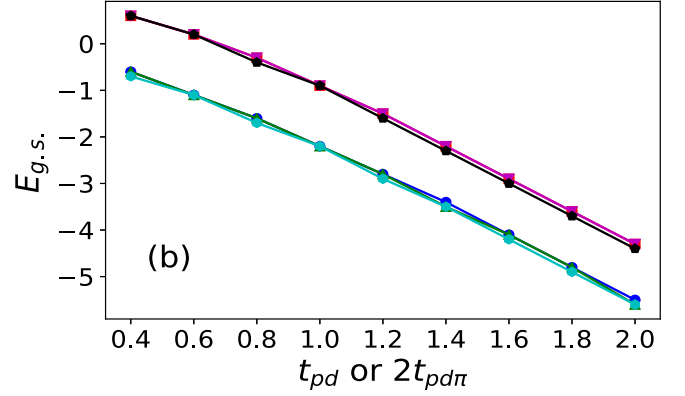
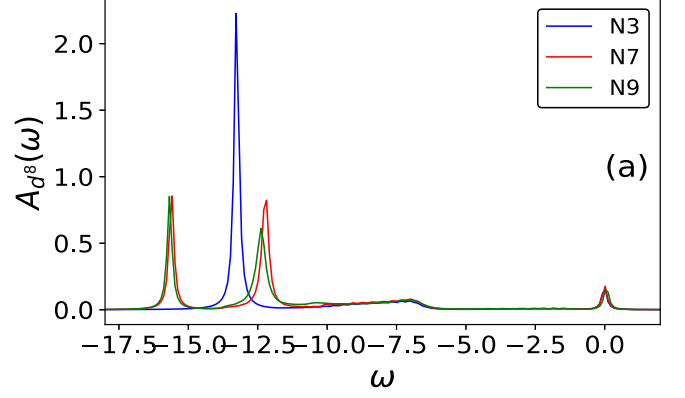


FIG. 6. (a) Comparison of two-hole spectra for the N3, N7, and N9 models. Parameters are $\Delta = 3.0$ eV, $A = 6.5$ eV, $U_{dd} = A + 4B + 3C = 8.84$ and $t_{pd} = 1.3$ eV, $t_{pp} = 0.65$ eV, $t_{pd\sigma} = 2.6/\sqrt{3}$ eV, $pd\pi = 0.65$ eV, $t_{pp\sigma} = 1.0$ eV, $t_{pp\pi} = 0.3$ eV; (b), (c) the ground-state energy and the weight of its corresponding peak as functions of the Cu-O hybridization t_{pd} and charge-transfer energy Δ .

IV. CONCLUSION

In summary, we used variational exact diagonalization to revisit the problem of the spectra of two holes doped into an otherwise full CuO_2 layer, modeled as a $\text{Cu-}d^{10}$ impurity properly embedded into a square lattice of O-2p⁶. While the relevance of the full Cu multiplet structure was considered before, with results in qualitative agreement with ours, we use a realistic tight-binding band structure for the O band and consider the implications of adding nonligand 2p orbitals as well.

Using a realistic O-2*p* band structure does not change qualitatively the two-hole spectra, compared to those obtained with a semielliptic one. However, there are significant quantitative changes: the region favoring a bound ground state with 1A_1 symmetry is enlarged significantly and extends well into the Mott-Hubbard region of the ZSA classification scheme. This proves that using a realistic band structure has nontrivial quantitative consequences, which are relevant if detailed modeling and comparison to experiments is desired. This is an important lesson for impurity-type calculations, including DMFT studies (if they use semielliptical bath densities of states instead of the correct bands).

Furthermore, we find that the three-band Emery model reproduces well the low-energy results obtained in the 1A_1 symmetry channel of the N7 and N9 models. Its ground state is consistent with the ZRS, but the overlap with the ZRS wave function is only around 50% for reasonable values of the parameters. This raises questions about the accuracy of projecting the Emery model onto ZRS, to obtain simple one-band Hamiltonians [14]. We point out again the importance of including all the multiplets when discussing energy scales larger than about 1 eV, as in many of the optical and photoemission spectroscopies. An obvious example is the appearance of the so-called “waterfall” feature [32] at energies of about 1 eV above the lowest-energy electron removal state. This can trivially be explained by taking into account all the multiplets and their hybridization with the oxygen bands, forming a broad region in energy where a huge number of bands cross and overlap so that a broad continuum sets in a momentum distribution plot of ARPES spectroscopy.

We also find that adding more O-2*p* orbitals (in the N9 and N11 models) has essentially no consequences on the 1A_1 symmetry low-energy spectra. All these results seem to confirm the validity of the conventional three-orbital Emery model for describing the low-energy physics. However, more care is needed before drawing that conclusion, as the Emery model completely misses the low-energy peaks of other symmetries that are revealed by the full calculation, and which may be relevant to various properties of the cuprates.

It is worth emphasizing that the projection onto different irreducible representations is only possible because we treat a single Cu impurity, as opposed to a lattice of Cu sites. To lowest order, these impurity bound states can be treated as electronic polarons and will attain a band structure, each with a small band width due to the large “effective mass” caused by the electronic dressing. This is similar to the dispersion of the ZR singlet states as obtained in the *t*-*J* or the *t*-*t'*-*t''*-*J* models [4]. In a fuller treatment of the full lattice, however, these various symmetries will mix everywhere in the Brillouin zone except at high-symmetry points, and thus it is questionable whether these states with other symmetries are truly irrelevant. In fact, the study by Lau [12] clearly demonstrates a strong ferromagnetic ordering of the two Cu spins sandwiching an oxygen hole. This is a strong indication that more extended cluster models need to be studied to check whether the influence of the magnetic order and of the hole or electron doping on the stability of the ZRS in single-band Hubbard model scenario is indeed valid in the doping region where superconductivity arises.

The lower symmetry of the lattice (as opposed to an impurity) may also explain how the *z*-axis polarization, discussed in the Introduction, may be accounted for. The $d_{3z^2-r^2}$, d_{xz} and d_{yz} orbitals have very little contribution to the 1A_1 ground state, but they contribute significantly to the low-energy peaks in the other symmetry channels. A lattice calculation that breaks the D_{4h} point-group symmetry may boost not only their contribution to the ground state, but also the importance of the O-2*p_z* orbitals that mostly hybridize with them.

To settle these questions, calculations for the lattice equivalent of the N7 model are needed. Needless to say, an exact solution is a very hard challenge. Instead, it may be possible to obtain accurate results using variational approximations similar to those used here, but extended to a full Cu lattice. We will investigate this next.

ACKNOWLEDGMENTS

This work was funded by Stewart Blusson Quantum Matter Institute, Natural Sciences and Engineering Research Council (NSERC) for Canada, and Canada First Research Excellence Fund (CFREF).

APPENDIX A: MORE DETAILS OF THE MODEL

Table I lists the Cu-O and O-O hopping integrals. We use the convention that the hybridization parameters t_{pd} , t_{pp} , $t_{pd\sigma}$, $t_{pd\pi}$, $t_{pp\sigma}$, $t_{pp\pi}$ are positive. The signs due to the orbitals’ overlap (see Fig. 1) are explicitly indicated.

Table II lists the interaction matrices for all singlet/triplet irreducible representations of the D_{4h} point group spanned by two *d* holes, in terms of the Racah parameters *A*, *B*, and *C*. As noted in the main text, the free-ion values $B = 0.15$ eV, $C = 0.58$ eV are adopted and *A* is treated as a variable in this work.

TABLE I. The Cu-O and O-O hopping integrals T_{nm}^{pd} and T_{nm}^{pp} with $m \in \{b_1(d_{x^2-y^2}), a_1(d_{3z^2-r^2}), b_2(d_{xy}), e_x(d_{xz}), e_y(d_{yz})\}$ for various models. The hoppings involving $p_{x_3}, p_{y_3}, p_{x_4}, p_{y_4}$ follow the sign convention illustrated in Fig. 1.

<i>m</i>	N3		N7		N9			
	$T_{mx_1}^{pd}$	$T_{my_2}^{pd}$	$T_{mx_1}^{pd}$	$T_{my_2}^{pd}$	$T_{mx_1}^{pd}$	$T_{my_1}^{pd}$	$T_{mx_2}^{pd}$	$T_{my_2}^{pd}$
b_1	$-t_{pd}$	t_{pd}	$-t_{pd}$	t_{pd}	$-\sqrt{3}t_{pd\sigma}/2$	0	0	$\sqrt{3}t_{pd\sigma}/2$
a_1			$t_{pd}/\sqrt{3}$	$t_{pd}/\sqrt{3}$	$-t_{pd\sigma}/2$	0	0	$-t_{pd\sigma}/2$
b_2					0	$t_{pd\pi}$	$t_{pd\pi}$	0
N11								
<i>m</i>	$T_{mx_1}^{pd}$	$T_{my_1}^{pd}$	$T_{mz_1}^{pd}$	$T_{mx_2}^{pd}$	$T_{my_2}^{pd}$	$T_{mz_2}^{pd}$		
b_1	$-\sqrt{3}t_{pd\sigma}/2$	0	0	0	$\sqrt{3}t_{pd\sigma}/2$	0		
a_1	$-t_{pd\sigma}/2$	0	0	0	$-t_{pd\sigma}/2$	0		
b_2	0	$t_{pd\pi}$	0	$t_{pd\pi}$	0	0		
e_x	0	0	$t_{pd\pi}$	0	0	0		
e_y	0	0	0	0	0	0	$t_{pd\pi}$	
N3/N7			N9/N11					
$T_{x_1y_2}^{pp}$	$2T_{x_1x_2}^{pp}$		$2T_{x_1y_2}^{pp}$		$2T_{x_2y_1}^{pp}$		$2T_{y_1y_2}^{pp}$	
t_{pp}	$t_{pp\pi}$	$t_{pp\sigma}$	$t_{pp\pi} + t_{pp\sigma}$	$t_{pp\pi} - t_{pp\sigma}$	$t_{pp\pi} + t_{pp\sigma}$	$t_{pp\pi} - t_{pp\sigma}$		

TABLE II. Irreducible representations spanned by two d holes (d^8) and corresponding Coulomb and exchange matrix elements in terms of Racah parameters A, B, C . The basis functions are based on the single-hole irreducible representations: $b_1(d_{x^2-y^2})$, $a_1(d_{3z^2-r^2})$, $b_2(d_{xy})$, $e_x(d_{xz})$, $e_y(d_{yz})$. Throughout the paper, the free-ion values $B = 0.15$ eV, $C = 0.58$ eV are adopted and A as a variable is also often referred to as Hubbard U , whose value varies in different materials.

1A_1	a_1^2	b_1^2	b_2^2	$(e_x^2 + e_y^2)/\sqrt{2}$
a_1^2	$A + 4B + 3C$	$4B + C$	$4B + C$	$\sqrt{2}(B + C)$
b_1^2	$4B + C$	$A + 4B + 3C$	C	$\sqrt{2}(3B + C)$
b_2^2	$4B + C$	C	$A + 4B + 3C$	$\sqrt{2}(3B + C)$
$(e_x^2 + e_y^2)/\sqrt{2}$	$\sqrt{2}(B + C)$	$\sqrt{2}(3B + C)$	$\sqrt{2}(3B + C)$	$A + 7B + 4C$
1A_2	b_1b_2	3B_1	a_1b_1	3B_2
b_1b_2	$A + 4B + 2C$	a_1b_1	$A - 8B$	a_1b_2
3A_2	b_1b_2	e_xe_y	1B_1	a_1b_1
b_1b_2	$A + 4B$	$6B$	a_1b_1	$(e_x^2 - e_y^2)/\sqrt{2}$
e_xe_y	$6B$	$A - 5B$	$(e_x^2 - e_y^2)/\sqrt{2}$	1B_2
1E	e_xb_1	e_xa_1	e_yb_2	e_yb_1
e_xb_1	$A + B + 2C$	$-\sqrt{3}B$	$-3B$	$A + B + 2C$
e_xa_1	$-\sqrt{3}B$	$A + 3B + 2C$	$-\sqrt{3}B$	$\sqrt{3}B$
e_yb_2	$-3B$	$-\sqrt{3}B$	$A + B + 2C$	$3B$
3E	e_xb_1	e_xa_1	e_yb_2	e_yb_1
e_xb_1	$A - 5B$	$-3\sqrt{3}B$	$3B$	$A - 5B$
e_xa_1	$-3\sqrt{3}B$	$A + B$	$-3\sqrt{3}B$	$3\sqrt{3}B$
e_yb_2	$3B$	$-3\sqrt{3}B$	$A - 5B$	$-3B$

APPENDIX B: VARIATIONAL EXACT DIAGONALIZATION

We summarize here our implementation of the variational exact diagonalization method that we use to calculate the propagator $G_d(m, z; \Gamma)$. The two-hole states in the variational space are of three possible types: (a) both holes are on the Cu; (b) one hole is on the Cu and one on an O; and (c) both holes are on O sites. All states in (a) are included in the variational space. For the (b) and (c) states, we impose a cutoff R_c between the O hosting the hole(s) and the Cu. Obviously, $R_c \rightarrow \infty$ recovers the full Hilbert space. We typically set $R_c = 20$ for the results shown below. This suffices for convergence to be reached for all the bound states. Unless we use a very large δ , the continua are not yet fully converged for this R_c , instead they look like a collection of peaks whose number increases with R_c . The upper and lower band edges are already converged, however, and that is all the information relevant for our analysis.

Within this variational space, we set up the Hamiltonian matrix for each irreducible representation and use standard exact diagonalization to calculate the corresponding propagators via Lanczos diagonalization.

APPENDIX C: WEAK DEPENDENCE OF PHASE DIAGRAM ON CHARGE-TRANSFER ENERGY Δ

Two-dimensional phase diagrams like those of Fig. 4 may be expected to change depending on whether the $A - \Delta$ axis is spanned by changing A while keeping Δ constant,

or by changing Δ while keeping A constant, or by some other protocol. In Fig. 7 we show how the phase diagram evolves with the charge-transfer energy Δ . The rather weak dependence of the $A - \Delta$ vs t_{pd} phase boundaries upon Δ confirms the importance of the energy separation between A and Δ . Specifically, as Δ governs the energy difference between the d^9 and $d^{10}L$ states, $A - \Delta$ governs the average energy difference between d^8 and d^9L . If A is less than Δ , we are closer to a Mott-Hubbard limit than a charge-transfer gap

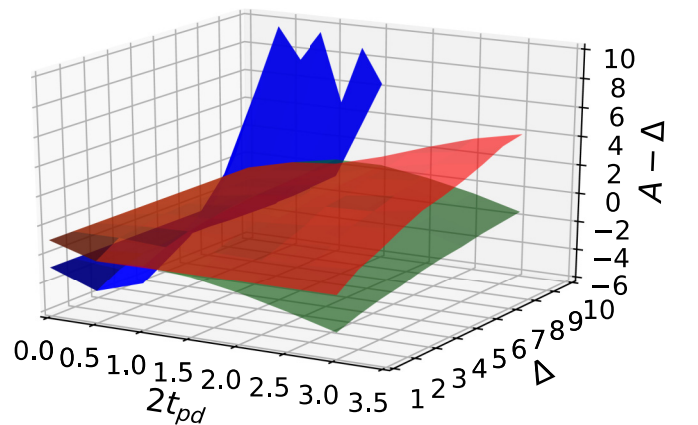


FIG. 7. Weak dependence of the phase boundaries of N7 phase diagram showed in Fig. 4(a) (with the same color conventions) on the charge-transfer energy Δ .

limit. In that case, the d^8 triplet is the lowest-energy electron removal state as clearly seen in Fig. 4, although the singlet

lowest-energy state extends well into this negative $A - \Delta$ region.

-
- [1] P. W. Anderson, *Science* **235**, 1196 (1987); G. Baskeran, Z. Zou, and P. W. Anderson, *Solid State Commun.* **63**, 973 (1987).
- [2] J. Zaanen, G. A. Sawatzky, and J. W. Allen, *Phys. Rev. Lett.* **55**, 418 (1985).
- [3] V. J. Emery, *Phys. Rev. Lett.* **58**, 2794 (1987).
- [4] F. C. Zhang and T. M. Rice, *Phys. Rev. B* **37**, 3759 (1988).
- [5] A. A. Aligia, M. E. Simón, and C. D. Batista, *Phys. Rev. B* **49**, 13061 (1994).
- [6] F. Lema and A. A. Aligia, *Phys. Rev. B* **55**, 14092 (1997).
- [7] I. Santoso, W. Ku, T. Shirakawa, G. Neuber, X. Yin, M. Enoki, M. Fujita, R. Liang, T. Venkatesan, G. A. Sawatzky, A. Kotlov, S. Yunoki, M. Rübhausen, and A. Rusydi, *Phys. Rev. B* **95**, 165108 (2017).
- [8] C. P. J. Adolphs, S. Moser, G. A. Sawatzky, and M. Berciu, *Phys. Rev. Lett.* **116**, 087002 (2016).
- [9] L. H. Tjeng, C. T. Chen, J. Ghijsen, P. Rudolf, and F. Sette, *Phys. Rev. Lett.* **67**, 501 (1991).
- [10] L. H. Tjeng, B. Sinkovic, N. B. Brookes, J. B. Goedkoop, R. Hesper, E. Pellegrin, F. M. F. de Groot, S. Altieri, S. L. Hulbert, E. Shekel, and G. A. Sawatzky, *Phys. Rev. Lett.* **78**, 1126 (1997).
- [11] N. B. Brookes, G. Ghiringhelli, O. Tjernberg, L. H. Tjeng, T. Mizokawa, T. W. Li, and A. A. Menovsky, *Phys. Rev. Lett.* **87**, 237003 (2001).
- [12] B. Lau, M. Berciu, and G. A. Sawatzky, *Phys. Rev. Lett.* **106**, 036401 (2011).
- [13] H. Ebrahimjad, G. A. Sawatzky, and M. Berciu, *Nat. Phys.* **10**, 951 (2014).
- [14] H. Ebrahimjad, G. A. Sawatzky, and M. Berciu, *J. Phys.: Condens. Matter* **28**, 105603 (2016).
- [15] H. Eskes and G. A. Sawatzky, *Phys. Rev. Lett.* **61**, 1415 (1988).
- [16] H. Eskes, L. H. Tjeng, and G. A. Sawatzky, *Phys. Rev. B* **41**, 288 (1990).
- [17] J. Zaanen and G. A. Sawatzky, *Can. J. Phys.* **65**, 1262 (1987).
- [18] F. M. F. de Groot, J. C. Fuggle, B. T. Thole, and G. A. Sawatzky, *Phys. Rev. B* **42**, 5459 (1990).
- [19] L. F. Feiner, M. Grilli, and C. Di Castro, *Phys. Rev. B* **45**, 10647 (1992).
- [20] A. Bianconi, P. Castrucci, A. Fabrizi, M. Pompa, A. M. Flank, P. Lagarde, H. Katayama-Yoshida, and G. Calestani, *Phys. C (Amsterdam)* **162–164**, 209 (1989); in *Earlier and Recent Aspects of Superconductivity*, edited by J. G. Bednorz and K. A. Muller, Springer Series in Solid State Sciences Vol. 90 (Springer, Berlin, 1990), p. 407.
- [21] A. Bianconi, in *Proceedings of the International Conference on Superconductivity-ICSC, Bangalore, 1990*, edited by S. K. Joshi, C. N. R. Rao, and S. V. Subramanyam (World Scientific, Singapore, 1990), p. 448.
- [22] H. Romberg, N. Nucker, M. Alexander, J. Fink, D. Hahn, T. Zetterer, H. H. Otto, and K. F. Renk, *Phys. Rev. B* **41**, 2609 (1990).
- [23] N. Nucker, H. Romberg, X. X. Xi, J. Fink, B. Gegenheimer, and Z. X. Zhao, *Phys. Rev. B* **39**, 6619 (1989).
- [24] W. Weber, *Z. Phys. B* **70**, 323 (1988).
- [25] D. L. Cox, M. Jarrell, C. Jayaprakash, H. R. Krishna-murthy, and J. Deisz, *Phys. Rev. Lett.* **62**, 2188 (1989).
- [26] M. Grilli, C. Castellani, and C. Di Castro, *Phys. Rev. B* **42**, 6233 (1990).
- [27] O. Tjernberg, L. H. Tjeng, P. G. Steeneken, G. Ghiringhelli, A. A. Nugroho, A. A. Menovsky, and N. B. Brookes, *Phys. Rev. B* **67**, 100501(R) (2003).
- [28] H. Sakakibara, H. Usui, K. Kuroki, R. Arita, and H. Aoki, *Phys. Rev. B* **85**, 064501 (2012).
- [29] C. E. Matt, D. Sutter, A. M. Cook, Y. Sassa, M. Månsson, O. Tjernberg, L. Das, M. Horio, D. Destraz, C. G. Fatuzzo *et al.*, *Nat. Commun.* **9**, 972 (2018).
- [30] W. M. Li, J. F. Zhao, L. P. Cao, Z. Hu, Q. Z. Huang, X. C. Wang, Y. Liu, G. Q. Zhao, J. Zhang, Q. Q. Liu, R. Z. Yu, Y. W. Long, H. Wu, H. J. Lin, C. T. Chen, Z. Li, Z. Z. Gong, Z. Guguchia, J. S. Kim, G. R. Stewart, Y. J. Uemura, S. Uchida, and C. Q. Jin, *PNAS* **116**, 12156 (2019).
- [31] G. A. Sawatzky and A. Lenselink, *Phys. Rev. B* **21**, 1790 (1980).
- [32] J. Graf, G.-H. Gweon, and A. Lanzara, *Phys. C (Amsterdam)* **460–462**, 194 (2007).
- [33] J. C. Slater and G. F. Koster, *Phys. Rev.* **94**, 1498 (1954).
- [34] M. Cini, *Solid State Commun.* **24**, 681 (1977); G. A. Sawatzky, *Phys. Rev. Lett.* **39**, 504 (1977).
- [35] We adopt the values in Fig. 2 of Ref. [16] for the ligand field splittings. Note that the precise values do not modify the implication in the text.
- [36] C. J. Ballhausen, *Introduction to Ligand Field Theory*, McGraw-Hill Series in Advanced Chemistry (McGraw-Hill, New York, 1962).
- [37] This is important because it means that the use Wannier functions and renormalized A, B, C Racah parameters to obtain the Hund's rule splittings starting from the atomic limit will not yield anything reasonable: to get the correct singlet triplet crossing, we would need to have a $J_h < 0$.
- [38] It is worth noting that this strong wave-function mixing is strongly dependent on t_{pd} , which in turn is strongly dependent on the interatomic distance between Cu and the nearest-neighbor O. This is the origin of a possibly strong electron-phonon and magnon-phonon coupling.